PNAS RESEARCH ARTICLE | PHYSIOLOGY

Actions of the antiseizure drug carbamazepine in the thalamic reticular nucleus: Potential mechanism of aggravating absence seizures

Sung-Soo Jang[a], Nicole Agranonik[a], and John R. Huguenard[a,1]

Edited by Moses Chao, New York University Langone Medical Center, New York, NY; received February 10, 2025; accepted June 23, 2025

Carbamazepine (CBZ) is a widely used antiepileptic drug effective in managing partial and generalized tonic-clonic seizures. Despite its established therapeutic efficacy, CBZ has been reported to worsen seizures in another form of epilepsy, generalized absence seizures, in both clinical and experimental settings. In this study, we focused on thalamic reticular (RT) neurons, which regulate thalamocortical network activity in absence seizures, to investigate whether CBZ alters their excitability, thereby contributing to the exacerbation of seizures. Using ex vivo whole-cell patch-clamp electrophysiology, we found that CBZ selectively inhibits the tonic firing of RT neurons in a dose-dependent manner without affecting burst firing. At the RT-thalamocortical synapse, CBZ significantly increases the failure rate of GABAergic synaptic transmission, with greater effects on somatostatin–than parvalbumin-expressing RT neurons. In vivo EEG recordings and open-field behavior in Scn8a $^{med\pm}$ mouse model confirmed that CBZ treatment exacerbates absence seizures, increasing both seizure frequency and duration while reducing locomotor activity. In addition, CBZ further amplifies the preexisting reduction in tonic firing of RT neurons in Scn8a$^{med\pm}$ mice. These findings uncover a mechanism by which CBZ exacerbates absence seizures through selective inhibition of RT neuron excitability and disruption of GABAergic synaptic transmission. This work provides mechanistic insights into the paradoxical effects of CBZ and suggests potential avenues for optimizing epilepsy treatment strategies.

carbamazepine | thalamic reticular nucleus | absence seizure | NaV channels

Significance

This study addresses the clinical paradox in which Carbamazepine (CBZ), a widely prescribed antiepileptic drug, paradoxically aggravates absence seizures. Understanding the cellular mechanisms behind this phenomenon is critical for improving epilepsy treatments. Here, using electrophysiology recordings from intact thalamocortical slices and SCN8a$^{med\pm}$ mice, an absence seizure animal model, we demonstrate that CBZ selectively inhibits tonic firing of RT neurons and their output to thalamocortical circuits, with a more pronounced effect in SCN8a$^{med\pm}$ mice. These findings provide a mechanistic explanation for CBZ's paradoxical aggravation of absence seizures, offering a framework for understanding the pharmacological effects of other antiepilepsy drugs and guiding the development of more effective therapeutic strategies for epilepsy.

Carbamazepine (CBZ) is widely prescribed for epilepsy management, effectively treating partial seizures, generalized tonic-clonic seizures, and mixed seizure patterns. Its primary mechanism of action is proposed to be suppression of repetitive neuronal firing through use-dependent blockade of voltage-gated sodium channels, thereby reducing seizure-related neuronal hyperactivity. However, clinical evidence indicates that CBZ exacerbates absence seizures (1–4) characterized by transient episodes of impaired consciousness and distinctive 3 Hz spike-and-wave discharge (SWD) on electroencephalography (EEG) in patients with generalized epilepsies. Studies in the Generalized Absence Epilepsy Rats from Strasbourg (GAERS) have documented that CBZ aggravates 3-6 Hz SWD through $GABA_A$ receptor-dependent mechanisms in the thalamic ventrobasal complex (VB) (5). In addition, CBZ has been shown to augment spontaneous SWDs in the stargazer mutant mouse model of absence seizures (6).

The thalamic reticular (RT) nucleus is a specialized structure composed of GABAergic neurons, serving as a major source of inhibition to thalamocortical (TC) neurons (7–9). Selective activation of RT neurons through optogenetic stimulation induces thalamocortical neuron burst firing and rhythmic activity, hallmark features of absence seizures (10). RT neurons are predominantly parvalbumin-expressing (PV), although recent studies have identified a subpopulation of somatostatin-positive (SOM) neurons within this nucleus (11). Notably, PV and SOM neurons differentially regulate distinct thalamocortical circuits. SOM-expressing RT neurons are implicated in the modulation of gamma rhythms and the processing of visual information in the primary visual cortex (V1) (12), whereas PV-expressing RT neurons contribute to rhythmic activity that underlies somatosensory behavior and the generation of absence seizures (11, 13, 14). Disruption of PV-expressing RT neuron activity is sufficient to induce spike-and-wave discharges (SWD) on an electroencephalogram (EEG) (13), highlighting their critical role in the pathophysiology of absence seizures. Hemizygous loss of *SCN8a*, which encodes the voltage-gated sodium channel Nav1.6, leads to reduced tonic firing of RT neurons and impaired intra-RT synaptic connectivity, contributing to thalamocortical network hypersynchrony and spontaneous absence seizures (15). Considering the central role of RT neurons in the modulation of absence seizures and the widespread use of CBZ in epilepsy treatment, it

Author affiliations: [a]Department of Neurology and Neurological Science, Stanford University, Stanford, CA 94305

Author contributions: S.-S.J. and J.R.H. designed research; S.-S.J. and N.A. performed research; J.R.H. contributed new reagents/analytic tools; S.-S.J., N.A., and J.R.H. analyzed data; S.-S.J. made the figures; and S.-S.J. and J.R.H. wrote the paper.

The authors declare no competing interest.

This article is a PNAS Direct Submission.

Copyright © 2025 the Author(s). Published by PNAS. This article is distributed under Creative Commons Attribution-NonCommercial-NoDerivatives License 4.0 (CC BY-NC-ND).

[1]To whom correspondence may be addressed. Email: John.Huguenard@stanford.edu.

This article contains supporting information online at https://www.pnas.org/lookup/suppl/doi:10.1073/pnas.2500644122/-/DCSupplemental.

Published July 31, 2025.

Downloaded from https://www.pnas.org by STANFORD UNIVERSITY on August 1, 2025 from IP address 171.66.11.105.

is important to understand whether CBZ influences electrophysiological properties within RT neurons, leading to the aggravation of absence seizure.

In this study, we show the following: 1) at clinically relevant concentrations (30 μM), CBZ selectively inhibits tonic firing without affecting burst firing of RT neurons; 2) CBZ increases the failure rate of GABAergic transmission at the RT-TC synapse, with greater effects observed in SOM-vs PV-expressing RT neurons; 3) In SCN8a$^{med\pm}$ mice, which exhibit spontaneous absence seizures, CBZ increases both seizure frequency and duration while inducing hypolocomotor activity; 4) CBZ inhibits RT excitability more prominently in SCN8a$^{med\pm}$ mice compared to SCN8a^{WT} mice. These findings enhance our understanding of the mechanisms underlying the paradoxical effect of CBZ in absence seizure, providing valuable insights for refining the therapeutic management of epilepsy.

Results

CBZ Selectively Inhibits Tonic Mode of RT Firing in an Activity-Dependent Manner. Given that CBZ has been shown to suppress sustained neuronal firing in a variety of cell types (16–19), we hypothesized that CBZ would have similar effects on RT neurons from the adolescent mice (P36-50). To test this hypothesis, we performed whole-cell patch clamp recordings on RT neurons using acute horizontal slices that preserved an intact thalamocortical circuit (Fig. 1*A*). RT neurons exhibited three distinct firing patterns: burst firing, burst followed by tonic firing, and tonic firing, elicited by weak, moderate, and strong membrane depolarization, respectively (Fig. 1*B*). We first examined the dose-dependent effects of CBZ on RT neuronal firing at concentrations of 20, 30, and 50 μM CBZ, which are within the therapeutic reference range (4 to 12 μg/mL) for humans (20, 21). Current-clamp recordings were performed using current steps from 0 to 210 pA for 1 s. CBZ inhibited action potential (AP) firing in a dose-dependent manner, which was fully recovered after a 15-min washout (*SI Appendix*, Fig. S1 *A–E*). We confirmed recovery in all findings, but for clarity these washout results are not included in all figures. AP responses were stable over time, and there were no detectable effects on passive membrane properties or individual AP kinetics in control conditions (*SI Appendix*, Fig. S2). CBZ did not change passive membrane properties (*SI Appendix*, Fig. S3*A*). These observations indicate that the observed effects of CBZ are not due to a run-down or deterioration of recording conditions but are instead specific to the drug treatment and its effects on APs. To further explore the mechanisms underlying CBZ's effects, we expanded the protocol to include depolarizing currents from 0 to 300 pA for 1 s (Fig. 1*C*). Given that 50 μM is near the top of the clinically relevant range (20), we selected a concentration of 30 μM (19), an effective dose with minimal evidence of side effects, for further study. Upon incubation with 30 μM CBZ for 10-min, we analyzed AP firing across three distinct time intervals within the spike train: early (0 to 100 ms, a period dominated by early burst firing), middle (500 to 600 ms, a period of transition between burst and tonic firing), and late (900 to 1,000 ms, a period restricted to only tonic firing) (Fig. 1*C*). AP numbers were significantly reduced by CBZ only during the middle and late time periods, while AP firing during the early period remained unaffected (Fig. 1*D*). We next investigated the effects of CBZ on fundamental AP properties including overshoot (mV), fast AHP (mV), Half-width (ms), AP threshold (mV), and AP amplitude (mV) in APs from the first 3 spikes and the last 3 spikes of each spike train. Comparisons between the first 3 and last 3 spikes in the spike train revealed significant CBZ-induced alterations in the AP properties, especially of the last 3 spikes (*SI Appendix*, Fig. S3 *B* and *C*). Phase-plane analysis of the somatic AP waveform further supported these findings, demonstrating changes in AP rise and fall rates (Max dV/dt, Min dV/dt) and axon initial segment (AIS)-to-soma propagation (1st and 2nd d^2V/dt^2 peaks) for the last 3 but not the first 3 spikes (Fig. 1*E*). Based on these observations, we hypothesized that CBZ selectively targets late tonic firing through a use-dependent block mechanism while sparing early burst firing. To test directly for an effect of CBZ on tonic firing, we held the membrane potential at –60 mV to inactivate T-type calcium channels, minimizing their contribution to spike generation, and thus reducing burst firing. Under these conditions, CBZ inhibited AP firing across all current steps (30 to 300 pA) (*SI Appendix*, Fig. S4 *A* and *B*) and time intervals (0 to 100, 500 to 600, and 900 to 1,000 ms) (*SI Appendix*, Fig. S4*C*) and affected key AP properties, including overshoot, half-width, and AP amplitude (*SI Appendix*, Fig. S4*D*). Last, based on the fact that CBZ can act in part via inhibiting L-type voltage gated calcium channel (22) which are also expressed in the soma of neurons in the reticular nucleus of the thalamus (23), and that T-type channels promote regenerative AP burst firing in reticular neurons (7), we investigated whether the effect of CBZ on tonic firing might be due in part to blockade of L-type or T-type calcium channels. The effects of CBZ on tonic firing persisted in the presence of nimodipine, a L-type calcium channel blocker (*SI Appendix*, Fig. S5 *A* and *B*) and Z944, a novel T-type calcium channel blocker (24) (*SI Appendix*, Fig. S5 *C* and *D*), suggesting that the effect of CBZ on tonic firing is not influenced by the inhibition of L-type and T-type calcium channels. Collectively, these findings highlight that CBZ selectively modulates RT neuronal excitability, with pronounced effects on tonic firing patterns, especially with depolarized resting membrane potentials.

CBZ Disrupts GABAergic Transmission at the RT-TC Synapse. To evaluate the effect of CBZ on synaptic output at RT to TC synapses, we utilized VGAT-ChR2 mice (VGAT-mhChR2-YFP), in which GABAergic neurons, including RT neurons, express channelrhodopsin-2 (ChR2) coupled with enhanced yellow fluorescent protein (hChR2-eYFP). Optogenetic stimulation using a 470 nm LED light reliably evoked postsynaptic currents (PSCs) in TC neurons under conditions where glutamatergic transmission was blocked by 1 mM kynurenic acid (Fig. 2*A*). To confirm whether PSCs in TC neurons are inhibitory currents, we recorded optogenetically evoked PSCs at different holding potentials between –70 and +40 mV while using a high-chloride internal solution. Polarity of evoked PSCs was reversed between –70 and +40 mV and the PSCs were abolished at –5 mV, the estimated chloride reversal potential (Fig. 2 *B*, *Left*). To further verify the inhibitory nature of these currents, we applied gabazine (SR-95531), a $GABA_A$ receptor antagonist, which completely eliminated the PSCs. These results confirm that the PSCs elicited by optogenetic stimulation in TC neurons are synaptic $GABA_A$ receptor-mediated chloride currents (Fig. 2*B*, left dark red trace, and right). Next, to investigate how CBZ affects GABAergic synaptic transmission at RT to TC synapses, we applied 470 nm LED stimulation at frequencies of 5, 10, 20, 30, and 50 Hz for 5 s. CBZ significantly increased the failure rate of inhibitory postsynaptic currents (IPSCs) in TC neurons with effects most prominent at 30 Hz (Fig. 2*C*). To further explore the mechanism underlying the increased failure rate, we analyzed synaptic latency—the interval between the onset of light stimulation and the onset of IPSCs during individual events over 5 s. Detailed analysis revealed that CBZ increased synaptic latency (Fig. 2*D* and *SI Appendix*, Fig. S6 *A* and *C*), consistent with an inhibitory CBZ effect on AP generation

Downloaded from https://www.pnas.org by STANFORD UNIVERSITY on August 1, 2025 from IP address 171.66.11.105.

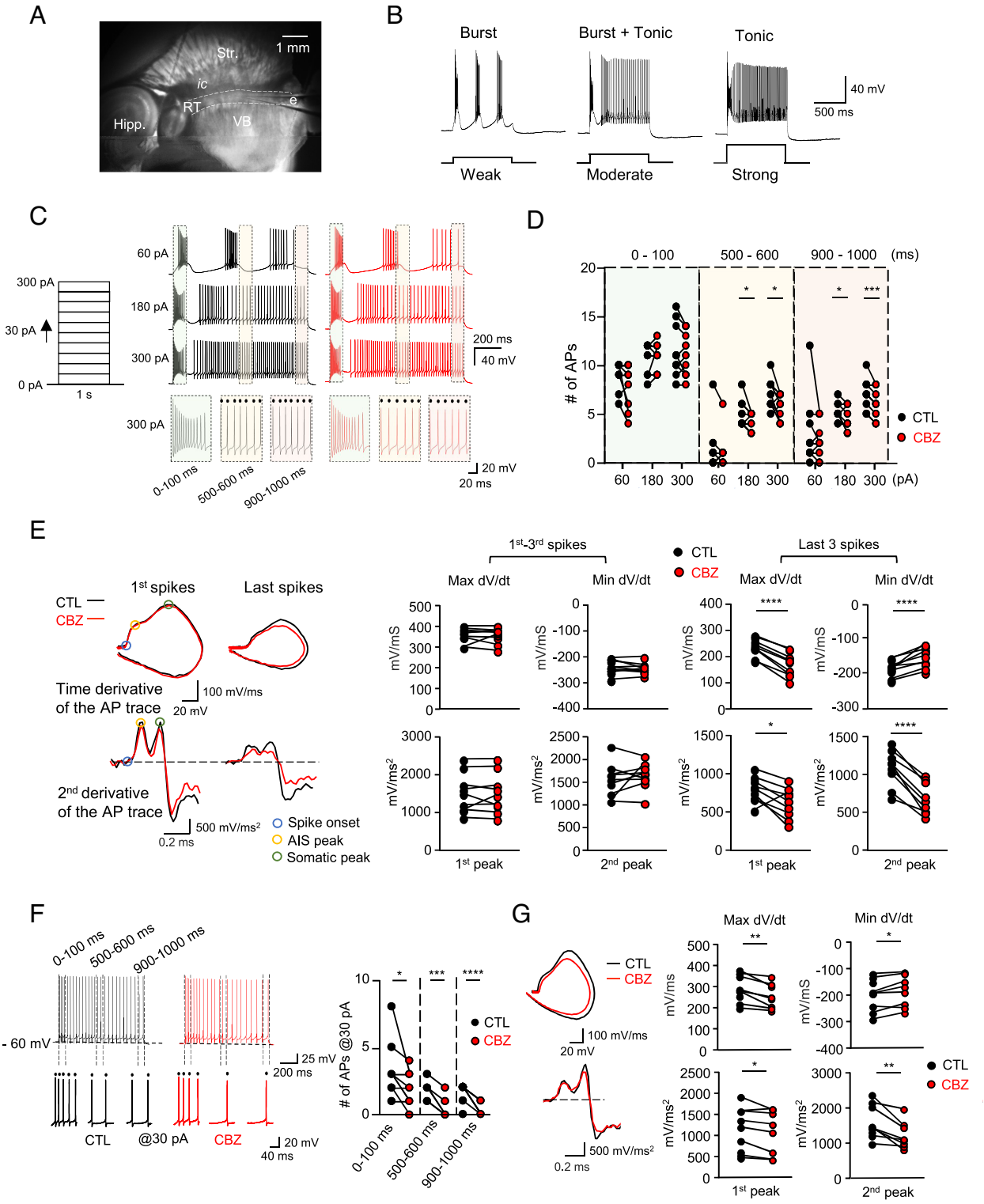


Fig. 1. Selective Inhibition of Tonic Firing in RT Neurons by CBZ. (*A*) Representative microscopic image of a horizontal brain slice (270 μm thickness) showing RT region and adjacent ventrobasal complex (VB). (*B*) Representative traces of action potentials (APs) illustrating two distinct firing modes in RT neurons: burst firing and tonic firing, elicited by weak, moderate, and strong depolarizing current injections, respectively. (*C*) Stimulation protocol (*Left*) and corresponding AP traces (*Right*) in RT neurons during a 1-s stimulation with increasing current injections (0 to 300 pA in 30 pA increments) before (black) and after (red) a 10-min incubation with 30 μM CBZ. Light green, light yellow, and light orange shaded areas highlight the first 100 ms, the 500 to 600 ms, and the final 100 ms of the stimulation epoch, respectively. Individual dots indicate single APs. (*D*) Graph showing the number of APs at specified time intervals (0 to 100 ms, 500 to 600 ms, 900 to 1,000 ms) in response to current injections of 60, 180, and 300 pA, as color-coded in (*C*). Individual cells are represented by filled circles (n = 9). (*E*) Representative traces (*Left*) showing the first derivative (dV/dt) and second derivative (d^2V/dt^2) waveforms of the first spike and last spike recorded at 300 pA and graph showing quantification (*Right*) of the average maximum and minimum dV/dt, as well as the first and second peaks of d^2V/dt^2, between the first three and last three APs at 300 pA, before (black) and after (red) a 10-min CBZ incubation (n = 9). (*F*) Representative traces (*Left*) and graph (*Right*) showing the number of spikes during tonic firing induced by 30 pA current injection from a holding potential of –60 mV, over a 1-s epoch, before (black) and after (red) a 10-min CBZ incubation (n = 9). Individual spikes are represented by black dots. (*G*) Representative traces (*Left*) showing the first derivative dV/dt (*Top*) and the second derivative d^2V/dt^2 (*Bottom*) waveforms for the first APs during tonic firing at 30 pA and graph (*Right*) showing average dV/dt, d^2V/dt^2, and their respective peaks between the first three APs at 30 pA before (black) and after (red) CBZ incubation. The paired *t* test was used for statistical analysis. **P* < 0.05, ***P* < 0.01, ****P* < 0.001, *****P* < 0.0001.

Downloaded from https://www.pnas.org by STANFORD UNIVERSITY on August 1, 2025 from IP address 171.66.11.105.

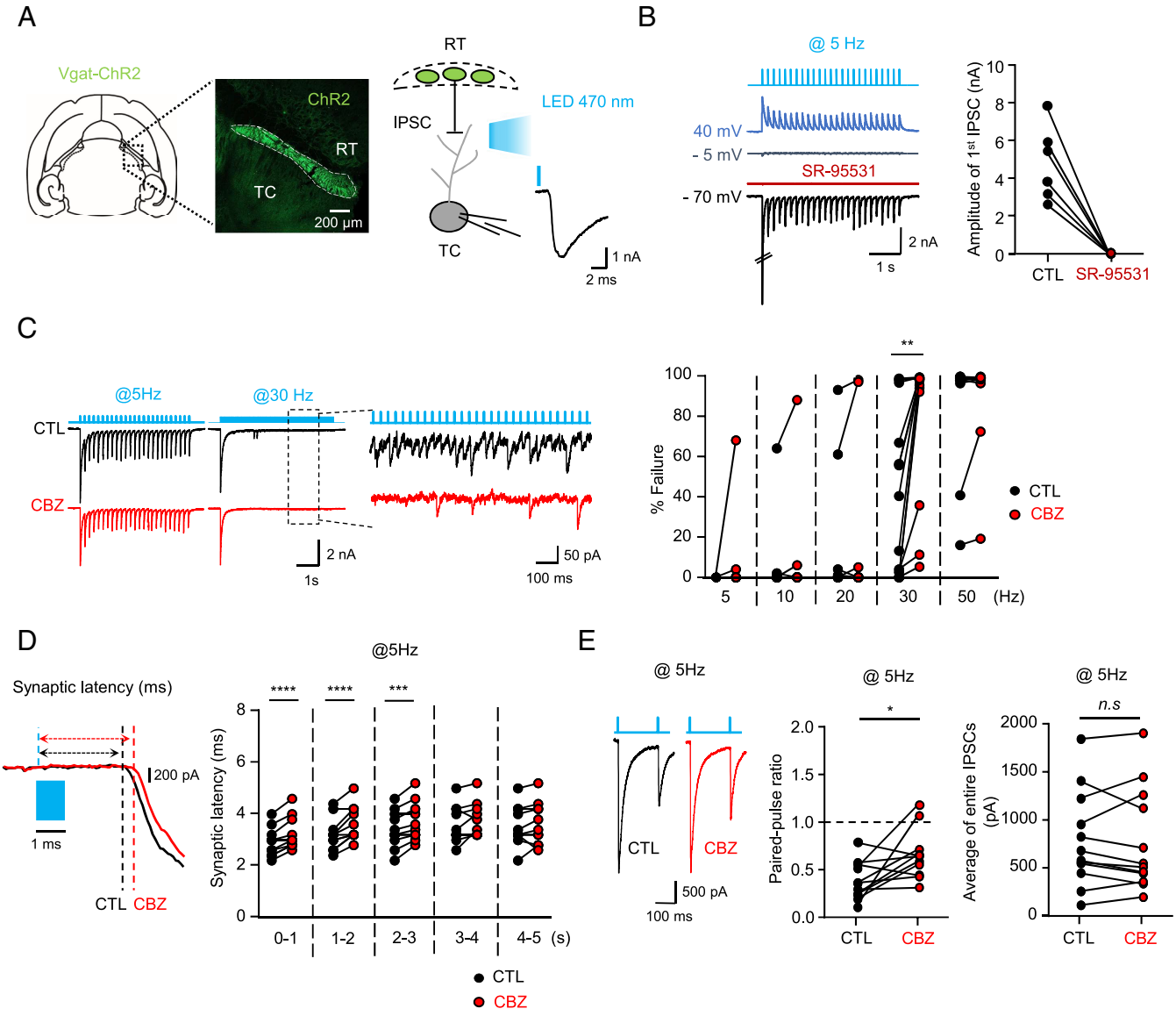


Fig. 2. Disruption of GABAergic Transmission at the RT-TC Synapse by CBZ. (*A*) Representative fluorescence images (*Left*) showing RT region expressing ChR2-YFP in VGAT-ChR2-EYFP mice, with a schematic (*Right*) illustrating the RT-TC synaptic circuit. Optogenetic activation of RT neurons was achieved with a 1 ms blue light pulse, while 1 mM kynurenic acid was applied to block glutamatergic transmission, isolating GABAergic inhibitory postsynaptic currents (IPSCs) in thalamocortical (TC) neurons. (*B*) Representative traces (*Left*) showing IPSCs in TC neurons evoked by 5 Hz optogenetic stimulation at different holding potentials (−70, −5, and 40 mV) and with SR-95531 (dark red trace, −70 mV), a $GABA_A$ receptor antagonist and graph (*Right*) showing amplitude of the 1st IPSC in response to 5 Hz optogenetic stimulation before and after SR-95531. (*C*) Representative traces (*Left*) showing IPSCs evoked in TC neurons by 5 Hz and 30 Hz optogenetic stimulation for 5 s and graph (*Right*) showing the percentage of synaptic failures in RT-TC inhibition across various stimulation frequencies (5, 10, 20, 30, and 50 Hz) before and after CBZ treatment (n = 12). (*D*) Representative traces (*Left*) showing synaptic latency (in ms) between optogenetic stimulation onset and IPSC onset during 5 Hz stimulation and graph (*Right*) showing quantified synaptic latency at 1-s intervals before and after CBZ treatment (n = 12). (*E*) Representative traces (*Left*) showing the 1st and 2nd IPSCs during 5 Hz stimulation, graph (*Middle*) showing the PPR, calculated as the ratio of the 2nd to the 1st IPSC peak amplitudes and graph (*Right*) displaying the average of entire IPSCs during 5 Hz stimulation before and after CBZ incubation. Statistical significance was determined using a paired *t* test. ***P* < 0.01, ****P* < 0.001, *****P* < 0.0001.

and propagation in RT axons. Last, we analyzed the paired-pulse ratio (PPR) of IPSCs during 5, 10, and 20 Hz stimulation. Our analysis revealed that CBZ significantly increased the PPR at low (5 Hz) frequencies (Fig. 2*E* and *SI Appendix,* Fig. S6 *B* and *D*). This finding is consistent with CBZ-mediated reduction in AP propagation into presynaptic terminals, which would reduce the probability of release, and increase the PPR (24). Collectively, these findings suggest that CBZ inhibits $GABA_A$-mediated RT output onto TC neurons in a frequency-dependent manner.

PV-and SOM-Expressing RT Neurons Exhibit Distinct Sensitivity to CBZ at the RT-TC Synapse. Considering the distinct anatomical and functional connections of the PV-and SOM-expressing RT neurons to TC neurons, as well as their diverse roles in behavior (11–13, 22), we sought to determine whether CBZ differentially affects the outputs of these two RT neuron subtypes. To address this, we introduced Cre-dependent hChR2-EYFP into the RT region of juvenile mice (P24-35) carrying either a PV-Cre or a SOM-Cre transgene. Three weeks postinjection (> P45) robust TC cell IPSCs were observed, confirming reliable expression of hChR2 in RT neurons of PV-Cre and SOM-Cre mice (Fig. 3*A*). The IPSCs recorded in SOM-Cre mice exhibited a higher failure rate compared to those in the PV-Cre mice during stimulation at 10, 20, and 30 Hz (Fig. 3*B*). CBZ further increased the IPSC failure rate during higher frequency stimulation in PV-Cre mice (30 and 50 Hz; Fig. 3*C*). Synaptic output from SOM-expressing

Downloaded from https://www.pnas.org by STANFORD UNIVERSITY on August 1, 2025 from IP address 171.66.11.105.

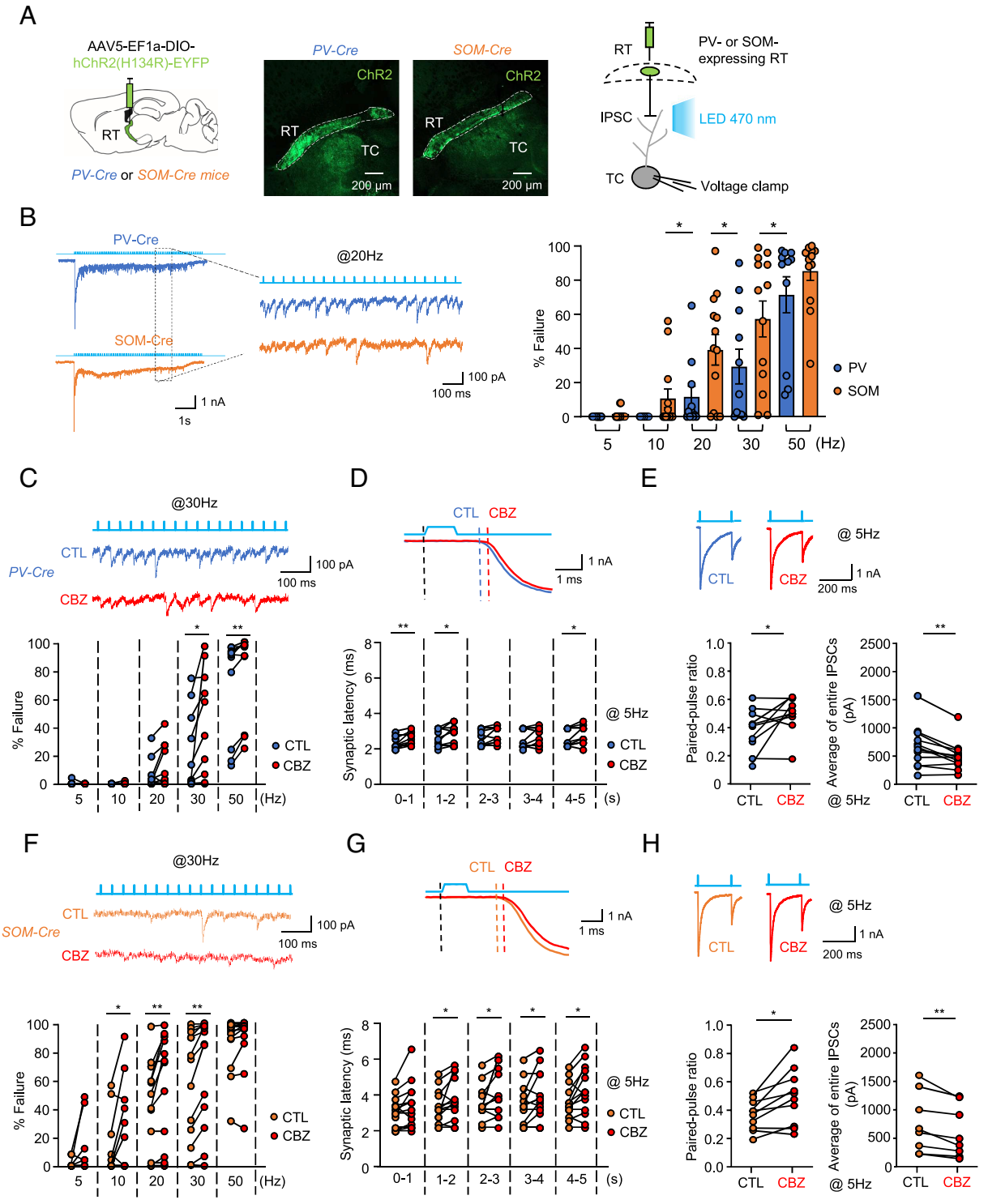


Fig. 3. Differential Sensitivity of GABAergic Transmission at PV-and SOM-Expressing RT-TC Synapses to CBZ. (*A*) Schematic (*Left*) illustrating the viral injection of AAV5-EF1a-DIO-hChR2(H134R)-EYFP into the RT region of PV-Cre and SOM-Cre mice, fluorescence images (*Middle*) of horizontal brain sections showing ChR2-EYFP (green) expression in RT neurons and schematic (*Right*) illustrating isolated RT synaptic connections to TC neurons and optogenetic activation of ChR2-expressing RT neurons in PV-Cre and SOM-Cre mice. (*B*) Representative traces (*Left*) and graph (*Right*) showing the percentage of IPSC failures in TC neurons from PV-Cre and SOM-Cre mice during optogenetic stimulation at 5, 10, 20, 30, and 50 Hz (PV-Cre: n = 10, SOM-Cre: n = 13). (*C*) Representative IPSC traces (*Top*) in PV-Cre mice during 30 Hz stimulation and graph (*Bottom*) showing the percentage of IPSC failures at the RT-TC synapse in PV-Cre mice across different stimulation frequencies (5, 10, 20, 30, and 50 Hz) before and after CBZ incubation (n = 10). (*D*) Representative traces (*Top*) of synaptic latency (ms) in PV-Cre mice during 5 Hz stimulation and graph (*Bottom*) showing synaptic latency between optogenetic stimulation onset and IPSC onset at 1-s intervals before and after CBZ incubation (n = 10). (*E*) Representative traces (*Top*) showing the 1st and 2nd IPSCs in PV-Cre mice during 5 Hz stimulation, graph (*Bottom*, *Left*) displaying the PPR, calculated as the ratio of the 2nd to 1st IPSC peak amplitudes, and graph (*Bottom*, *Right*) displaying the average of entire IPSCs during 5 Hz stimulation before and after CBZ incubation. (*F*) Representative IPSC traces (*Top*) in SOM-Cre mice during 30 Hz stimulation and graph (*Bottom*) showing the percentage of IPSC failures at the RT-TC synapse in SOM-Cre mice across different stimulation frequencies (5, 10, 20, 30, and 50 Hz) before and after CBZ incubation (n = 13). (*G*) Representative traces (*Top*) showing synaptic latency (ms) in SOM-Cre mice during 5 Hz stimulation and graph (*Bottom*) showing synaptic latency between optogenetic stimulation onset and IPSC onset at 1-s intervals before and after CBZ incubation (n = 13). (*H*) Representative traces (*Top*) showing the 1st and 2nd IPSCs in SOM-Cre mice during 5 Hz stimulation, graph (*Bottom*, *Left*) displaying the PPR, calculated as the ratio of the 2nd to 1st IPSC peak amplitudes, and graph (*Bottom*, *Right*) displaying the average of entire IPSCs during 5 Hz stimulation before and after CBZ incubation. Statistical significance was determined using a paired *t* test. **P* < 0.05, ***P* < 0.01.

Downloaded from https://www.pnas.org by STANFORD UNIVERSITY on August 1, 2025 from IP address 171.66.11.105.

RT neurons was more strongly affected by CBZ, with elevated failure rate at lower frequencies (10, 20, and 30 Hz; Fig. 3*F*). CBZ significantly impacted synaptic latency at both PV-and SOM-expressing RT to TC synapses during 5 Hz stimulation (Fig. 3 *D* and *G*), and at higher frequencies of 10 and 20 Hz (*SI Appendix,* Fig. S7 *A* and *D*). At both PV-and SOM-expressing RT to TC synapses, CBZ significantly increased the PPR, consistent with earlier results with VGAT-ChR2 mice (Fig. 2*E*) during 5 Hz stimulation (Fig. 3 *E* and *H*), but not at 10 or 20 Hz (*SI Appendix,* Fig. S7 *A–D*). Together, these findings suggest that CBZ exerts subtype-specific and frequency-dependent effects on RT to TC synaptic transmission, highlighting the differential modulation of PV-and SOM-expressing RT neuron outputs by CBZ.

CBZ Aggravates Absence Seizure and Reduced Locomotor Activity in the Absence Seizure Model of SCN8a$^{med/+}$ Mice. Previous report indicates that CBZ aggravates absence seizures in GAERS (5) and in a mouse model of acute absence seizures induced by γ-butyrolactone (GBL) (6), both of which are accompanied by motor impairments including behavioral arrest (5, 6). Based on these findings, we hypothesized that CBZ might worsen deficits in locomotor activity in part through increases in behavioral absence seizures, in which locomotor activity pauses. To test this hypothesis, we utilized SCN8a$^{med/+}$ mice (> P40), which exhibit spontaneous absence seizures characterized by SWD that have been previously validated in our lab (15). EEG recordings confirmed the presence of SWDs in SCN8a$^{med/+}$ mice, a hallmark of absence seizures, which were ameliorated by ethosuximide (200 mg/kg), an antiabsence seizure medication (Fig. 4*A*, n = 3). In contrast, while SCN8a^{WT} mice displayed no abnormalities on EEG (*SI Appendix,* Fig. S8*A*), administration of a low dose of pentylenetetrazol (PTZ; 20 mg/kg) effectively induced SWDs in these SCN8a^{WT} mice (*SI Appendix,* Fig. S8 *A* and *B*). To investigate the effects of CBZ on SWDs, we administered either vehicle or CBZ (15 mg/kg, intraperitoneally) to both SCN8a^{WT} mice and SCN8a$^{med/+}$ mice and performed EEG recordings for 1 h. In SCN8a$^{med/+}$ mice, CBZ significantly increased the number and total duration of SWD during the 20 to 40 min period following injection compared to baseline (Fig. 4 *B–D*). We further evaluated general locomotor activity using the open field test, a standard assay for measuring travel distance (Fig. 4*E*). During the 20 to 30 min period following i.p injection, SCN8a$^{med/+}$ mice in both vehicle-and CBZ-treated groups exhibited significantly reduced travel distances compared to SCN8a^{WT} mice (Fig. 4 *F* and *G*). Strikingly, CBZ treatment further reduced travel distance of SCN8a$^{med/+}$ mice compared to the vehicle-injected groups during the 30 to 40 min postinjection period (Fig. 4 *F* and *G*). These results demonstrate that CBZ aggravates absence seizures and the reduction of locomotion observed in the SCN8a$^{med/+}$ mouse model of absence seizures, highlighting its deleterious effects on both seizure activity and locomotor behavior.

CBZ Aggravates the Preexisting Reduction of RT Firing in SCN8a$^{med/+}$ Mice. Previously, we reported that the reduced firing of RT neurons in SCN8a$^{med/+}$ mice contributes to the pathogenesis of absence seizures (15). To determine whether CBZ-induced aggravation of absence seizures in SCN8a$^{med/+}$ mice (Fig. 4 *C* and *D*) results from further inhibition of tonic firing of RT neurons, we recorded APs in RT neurons using a series of square pulses (0 to 300 pA in 30 pA increments) with the same concentration of CBZ (30 μM) applied in Fig. 1. Consistent with our prior findings (15), RT neurons in SCN8a$^{med/+}$ mice exhibited a lower number of APs compared to SCN8a^{WT} mice under control conditions, particularly in response to the strongest depolarizing current injections (300 pA) (Fig. 5*A*). CBZ significantly reduced the number of APs during the last 500 ms, comprising tonic firing, in both SCN8a^{WT} and SCN8a$^{med/+}$ mice (Fig. 5*B* and *SI Appendix,* Fig. S9*A*). Notably, this reduction in APs was significantly greater in SCN8a$^{med/+}$ mice compared to SCN8a^{WT} (Fig. 5*B*). AP properties during the first three spikes under 240 pA current injection were minimally affected by CBZ (*SI Appendix,* Fig. S10*A*). As observed previously (*SI Appendix,* Fig. S3 *B* and *C*), CBZ altered AP properties in SCN8a^{WT}, including overshoot, threshold, amplitude, half-width, maximum and minimum dV/dt, from the last three spikes (*SI Appendix,* Fig. S10*B*). However, these AP properties in SCN8a$^{med/+}$ mice were not significantly affected by CBZ. (*SI Appendix,* Fig. S10*B*). To assess the use-dependent effects of CBZ, particularly whether these effects were driven by steady depolarization during the train vs. just during the AP transient depolarization, we applied pulse train stimulation (300 pA, 5 ms per pulse) at frequencies of 5, 10, 20, 30, and 50 Hz for 5 s. These stimuli reliably induced single action potentials with each pulse (Fig. 5*C*). CBZ did not affect the number of APs generated during pulse trains at any tested frequency (Fig. 5 *D* and *E*). AP properties from the first three spikes and last three spikes in both SCN8a^{WT} and SCN8a$^{med/+}$ mice were not affected by CBZ (*SI Appendix,* Fig. S11 *A* and *B*). These findings show that CBZ aggravates the impairment of RT firing in SCN8a$^{med/+}$ mice specifically during maintained DC step current injections. Thus, the sustained depolarization between each action potential is critical and necessary to induce use-dependent block. Activity patterns with periods of sustained depolarizations during seizures would then presumably contribute to the CBZ-induced worsening of absence seizures.

CBZ Effects on GABAergic Transmission at RT-TC Synapses in SCN8a$^{med/+}$ Mice. Finally, we assessed whether the effects of loss of SCN8a would exacerbate the effects of CBZ on GABAergic transmission at RT-TC synapses. Initially, we confirmed that compared to SCN8a^{WT} mice, SCN8a$^{med/+}$ mice exhibit an increased failure rate at 20 Hz stimulation (Fig. 6*A*), with a nonsignificant difference in synaptic latency compared to controls (5 and 10 Hz stimulation, Fig. 6*B* and *SI Appendix,* Fig. S12*A*). Failures were seen in SCN8a$^{med/+}$ mice, even at low stimulus frequencies (5 and 10 Hz) that produced no failures in SCN8a^{WT} mice (Fig. 6*C*). The failure rates were quite variable from cell to cell in SCN8a$^{med/+}$ mice and we did observe consistent CBZ-induced effects (Fig. 6*C*). Consistent with previous findings (Fig. 2*D*), CBZ also increased synaptic latency in both genotypes (Fig. 6*D* and *SI Appendix,* Fig. S12*B*). Last, we analyzed the PPR and found no significant difference between SCN8a^{WT} and SCN8a$^{med/+}$ mice, nor any effect of CBZ on it (*SI Appendix,* Fig. S12 *C* and *D*). Collectively these findings indicate that CBZ does not further exacerbate inhibitory effects at the RT-TC synapse in SCN8a$^{med/+}$ mice.

Discussion

This study elucidates the potential mechanisms behind CBZ's paradoxical aggravation of absence seizures using electrophysiological and behavioral assessments. CBZ selectively inhibits the tonic firing mode in RT neurons in an activity-dependent manner and suppresses GABAergic transmission at the RT-TC synapse. In the SCN8a$^{med/+}$ mouse model, which exhibits spontaneous absence seizures due to reduced tonic firing in RT neurons (15), CBZ aggravates the preexisting reduction in tonic firing of RT neurons in SCN8a$^{med/+}$ mice, and increases both the number and duration of SWDs. These findings provide insights into the poorly

Downloaded from https://www.pnas.org by STANFORD UNIVERSITY on August 1, 2025 from IP address 171.66.11.105.

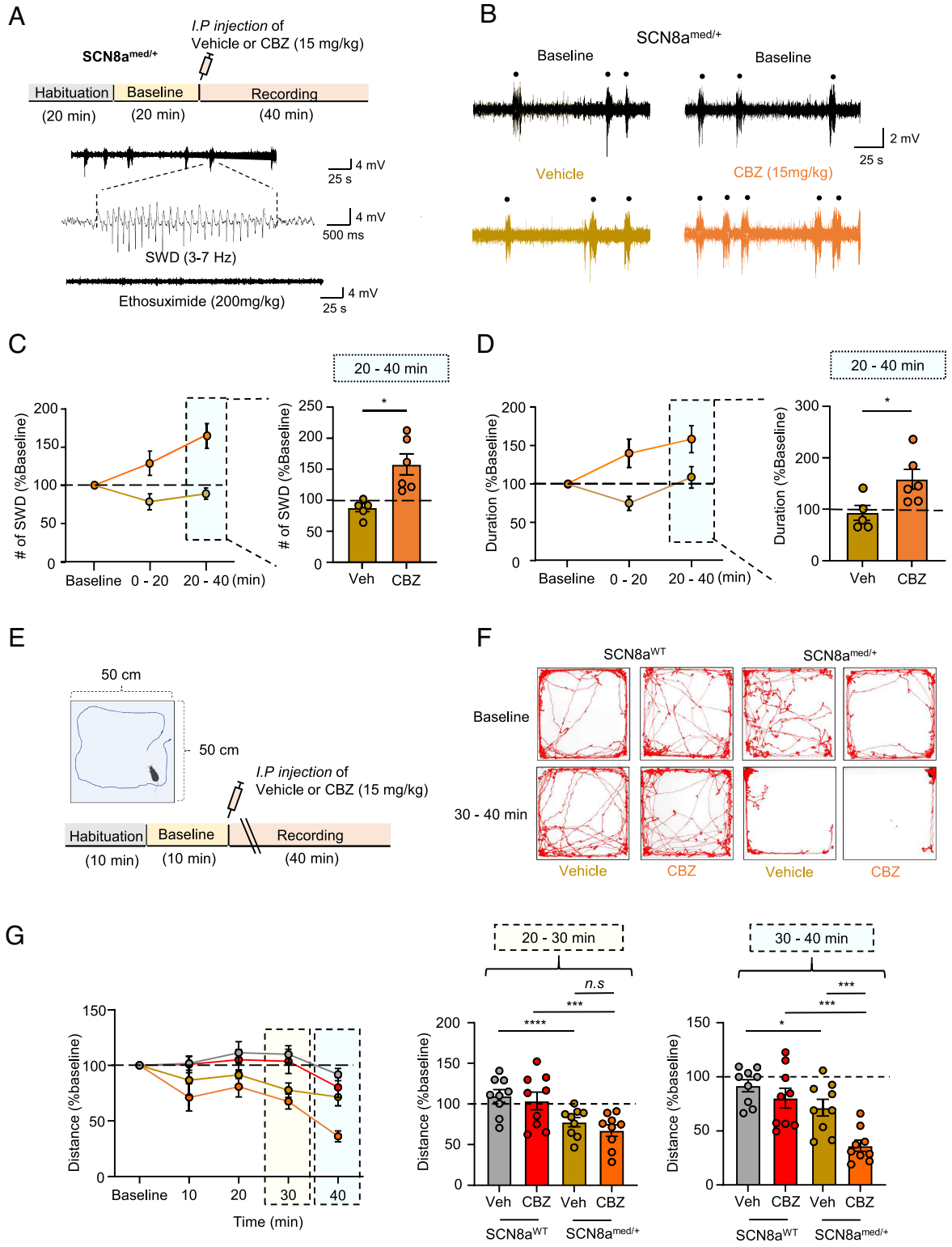


Fig. 4. Impact of CBZ on Absence Seizures and Hypoactivity in the Absence Seizure Model of SCN8a$^{med/+}$ Mice. (*A*) Experimental timeline (*Top*) outlining the protocol for habituation (20 min), baseline recording (20 min), and treatment (40 min). Representative EEG traces (*Bottom*) showing spike-wave discharges (SWDs, 3 to 7 Hz), characteristic of absence seizures, and the suppression of SWD activity following Ethosuximide administration (200 mg/kg, i.p.). (*B*) Representative EEG traces showing SWD activity during baseline, after either vehicle or CBZ administration (15 mg/kg, i.p.) in SCN8a$^{med/+}$ mice. (*C*) Graph (*Left*) showing the normalized number of SWDs over a 60-min recording period and graph (*Right*) showing the normalized number of SWDs during the 20 to 40 min postadministration period following either vehicle or CBZ (15 mg/kg, i.p.) in SCN8a$^{med/+}$ mice (Veh: n = 5, CBZ: n = 6). (*D*) Graph (*Left*) showing the normalized total duration of SWDs over 60 min and graph (*Right*) summarizing the normalized total duration of SWDs during the 20 to 40 min posttreatment period following vehicle or CBZ (15 mg/kg, i.p.) in SCN8a$^{med/+}$ mice (Veh: n = 5, CBZ: n = 6). (*E*) Experimental timeline outlining the protocol for habituation (10 min), baseline recording (10 min), and posttreatment recording (40 min) in the open field. (*F*) Representative movement traces showing locomotor activity in the open field during baseline and following vehicle or CBZ (15 mg/kg, i.p.) administration in SCN8a^{WT} and SCN8a$^{med/+}$ mice. (*G*) Graph (*Left*) showing the normalized distance traveled over 50 min during baseline and following vehicle or CBZ (15 mg/kg, i.p.) administration and graph (*Right*) showing the normalized distance traveled during the 20 to 30 min and 30 to 40 min intervals posttreatment with vehicle or CBZ (15 mg/kg, i.p.) in SCN8a^{WT} (Veh: n = 9, CBZ: n = 9) and SCN8a$^{med/+}$ mice (Veh: n = 9, CBZ: n = 9). Statistical significance was determined using a paired *t* test and two-way ANOVA with repeated measures. *P < 0.05, **P < 0.01, ***P < 0.001.

Downloaded from https://www.pnas.org by STANFORD UNIVERSITY on August 1, 2025 from IP address 171.66.11.105.

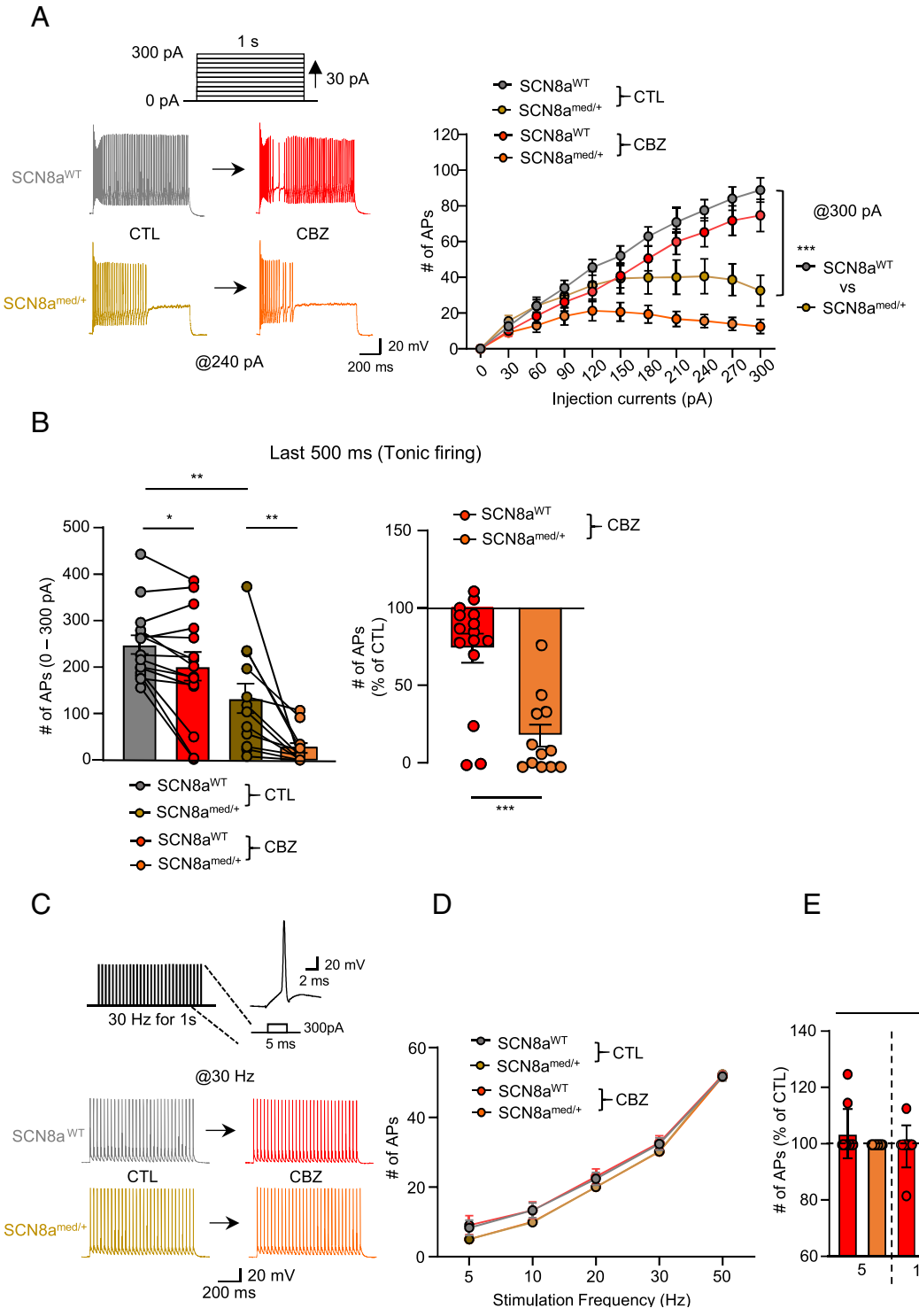


Fig. 5. Aggravated Inhibition of Tonic Firing in RT by CBZ in SCN8a$^{med/+}$ Mice. (*A*) Representative traces (*Left*) showing the number of APs elicited by 240 pA current injection for 1-s current injection in RT neurons before and after a 10-min incubation with CBZ in SCN8a^{WT} and SCN8a$^{med/+}$ mice and graph (*Right*) depicting the number of APs elicited by current injections ranging from 0 to 300 pA under CTL and CBZ conditions in SCN8a^{WT} (n = 15) and SCN8a$^{med/+}$ mice (n = 15). (*B*) Graph (*Left*) showing the total number of APs for last 500 ms elicited by 0 to 300 pA before and after a 10-min incubation with CBZ and graph (*Right*) showing the normalized number of APs to CTL in SCN8a^{WT} and SCN8a$^{med/+}$ mice. (*C*) Experimental design illustrating a pulse train (30 Hz) with 1-s 300 pA current injections (5 ms each) and representative traces (*Bottom*) of APs elicited by 30 Hz pulse trains before and after CBZ (30 μM) incubation in SCN8a^{WT} and SCN8a$^{med/+}$ mice. (*D*) Graph showing the number of APs elicited by 5, 10, 20, 30, and 50 Hz pulse trains under CTL and CBZ conditions in SCN8a^{WT} (n = 10) and SCN8a$^{med/+}$ mice (n = 9). (*E*) Graph showing the normalized number of APs to CTL in SCN8a^{WT} and SCN8a$^{med/+}$ mice at different frequencies (5, 10, 20, 30, and 50 Hz). Statistical significance was determined using a paired *t* test and two-way ANOVA with repeated measures. *$P < 0.05$, **$P < 0.01$, ***$P < 0.001$.

understood phenomenon of CBZ-induced worsening of absence seizures, shedding light on managing epilepsy treatment (Fig. 7).

CBZ is an effective anticonvulsant drug for adults and children with partial and secondarily generalized seizures (25, 26). In children, however, CBZ exacerbates certain seizure types, including absence, atonic, tonic, and myoclonic seizures (1, 4, 27, 28). This paradoxical effect has been explored in animal models, demonstrating that high-dose CBZ (25 mg/kg) aggravates absence seizures in γ-butyrolactone (GBL)-induced and stargazer mouse models (6). Similarly, intracerebroventricular (15 μg in 4 μL) and VB thalamic

Downloaded from https://www.pnas.org by STANFORD UNIVERSITY on August 1, 2025 from IP address 171.66.11.105.

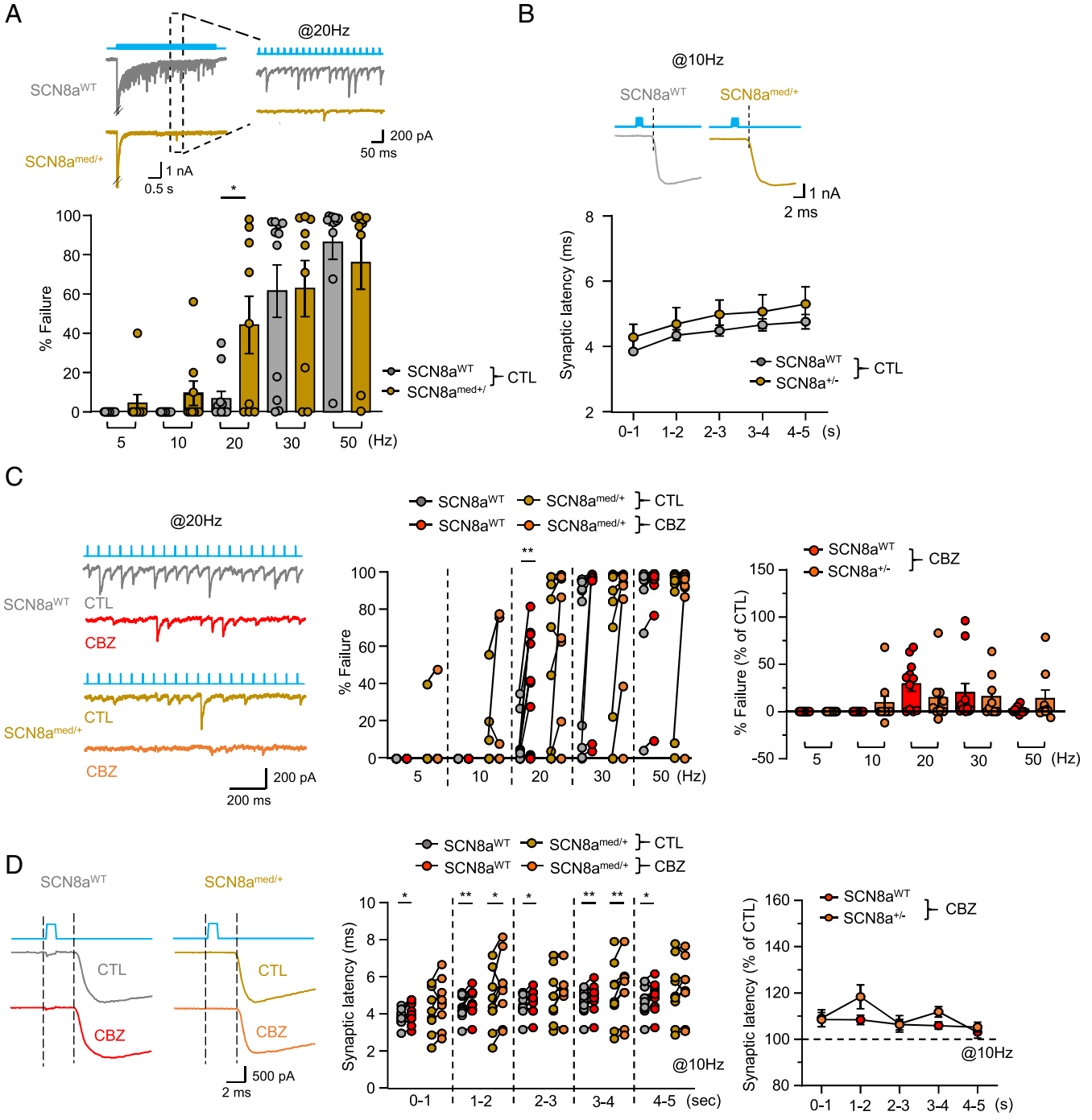


Fig. 6. Effects of CBZ on GABAergic Transmission at the RT-TC Synapse Between SCN8a^{WT} and SCN8a$^{med/+}$ Mice. (*A*) Representative traces (*Top*) showing inhibitory postsynaptic currents (IPSCs) in TC neurons evoked by 20 Hz optogenetic stimulation for 5 s and graph (*Bottom*) showing the percentage of failure in IPSCs at varying stimulation frequencies (5, 10, 20, 30, 50 Hz) in SCN8a^{WT} (n = 11) and SCN8a$^{med/+}$ mice (n = 9) expressing VGAT-ChR2-EYFP. (*B*) Representative traces (*Top*) showing synaptic latency between optogenetic stimulation and IPSC onset and graph (*Bottom*) showing quantified synaptic latency at 1-s intervals during 10 Hz stimulation in SCN8a^{WT} (n = 11) and SCN8a$^{med/+}$ mice (n = 9) expressing VGAT-ChR2-EYFP. (*C*) Representative traces (*Left*) showing IPSCs evoked by 20 Hz stimulation before and after CBZ incubation for 10 min, graph (*Middle*) showing the percentage of failure in IPSCs in response to optogenetic stimulations (5, 10, 20, 30, 50 Hz), and graph (*Right*) showing the normalized failure rates to CTL in SCN8a^{WT} (n = 11) and SCN8a$^{med/+}$ mice (n = 9). (*D*) Representative traces (*Left*) showing synaptic latency at 10 Hz stimulation before and after CBZ incubation for 10 min, graph (*Middle*) showing quantified synaptic latency at 1-s intervals, and graph (*Right*) showing the normalized latency to CTL in SCN8a^{WT} (n = 11) and SCN8a$^{med/+}$ mice (n = 9). Statistical significance was determined using a paired *t* test. *$P < 0.05$, **$P < 0.01$.

(0.75 μg in 0.2 μL) CBZ microinjections prolong seizure duration, effects that are blocked by the $GABA_A$ receptor antagonist bicuculline (5), implicating the involvement of GABA signaling pathways in CBZ-induced seizure aggravation. Given the central role of RT neurons as a GABAergic mediator of thalamic oscillatory activity (11, 14, 29), focusing the research on these GABAergic neurons enables a deeper understanding of this paradoxical phenomenon. In addition, it remains important to consider whether CBZ's effects in RT neurons vary across developmental stages, particularly during earlier postnatal periods. Although the developmental profiles of ion channels, including Nav channel expression, subunit composition, and inactivation properties during juvenile and adult stages are not well characterized in RT neurons, age-dependent changes could alter neuronal sensitivity to CBZ.

Downloaded from https://www.pnas.org by STANFORD UNIVERSITY on August 1, 2025 from IP address 171.66.11.105.

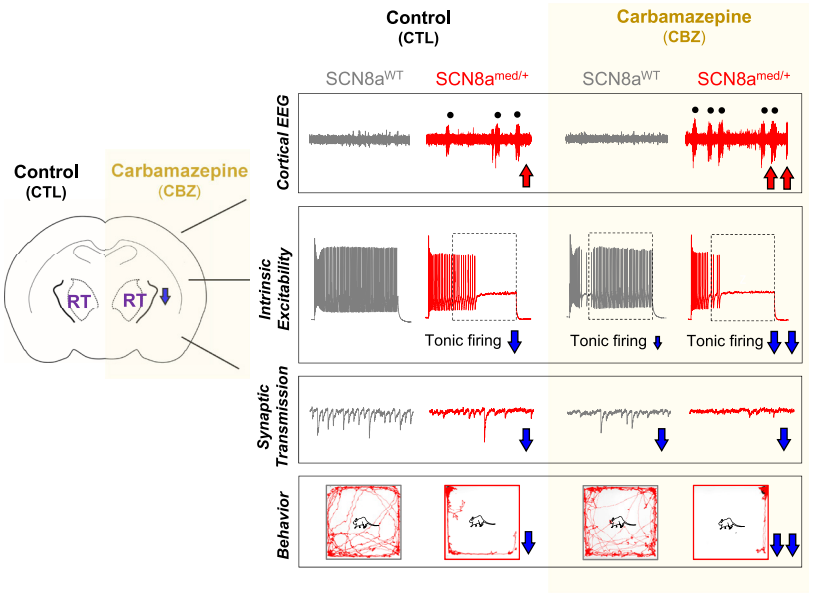


Fig. 7. Graphical abstract. CBZ selectively inhibits tonic, but not burst firing in RT neurons and disrupts GABAergic synaptic output at the RT-TC synapses. In SCN8a$^{med/+}$ mice, CBZ exacerbates absence seizures, increasing SWDs and reducing locomotor activity. In whole-cell patch clamp recordings, CBZ further suppresses tonic firing in RT neurons, but does not alter GABAergic transmission at RT-TC synapses. These findings provide a mechanistic explanation for the paradoxical seizure-aggravating effect of CBZ in absence epilepsy, highlighting dysfunction within the RT circuit.

To understand the relevance of these findings to human therapeutic outcomes, it is essential to compare the therapeutic concentration ranges in humans with the responses observed at corresponding concentrations in animal models. Studies in epileptic patients reported CBZ serum concentrations ranging from approximately 13 to 51 μM/L, within the therapeutic range. (30). Based on these data, we aimed to evaluate the effects of CBZ on RT neurons across a range of physiologically relevant concentrations (20, 30, and 50 μM). Our findings showed that 50 μM CBZ induced a 50% reduction in AP numbers in evoked spike trains, while 30 μM CBZ caused a moderate yet significant reduction in APs. This suggests that modest changes in baseline Nav function are sufficient to prevent seizures. To better understand the blocking mechanism of CBZ in RTs APs, we settled on 30 μM CBZ, a concentration that reliably produced detectable effects on AP generation (17, 19), yet was unlikely to be the toxic range in which side effects such as coma, respiratory failure, and cardiac conduction defects would be notable (31, 32). Given the impairment of RT excitability and GABAergic transmission at the RT-TC synapse in thalamic hypersynchrony and absence seizure (13, 15, 29, 33, 34) along with our observation that CBZ increased the number and total duration of SWD in SCN8a$^{med/+}$ mice, we propose that CBZ's inhibitory effect on RT excitability might underlie aggravation of absence seizure. CBZ inhibits voltage-dependent Na^+ channels through two primary mechanisms (35–38): 1) blocking Na^+ channels in their resting state at hyperpolarized membrane potentials and 2) inducing an activity-dependent block, an action enhanced during sustained depolarization. This results in a progressive reduction in spikes during high-frequency, but not low-frequency firing, supported by findings of enhanced CBZ inhibition of sodium channels in neuroblastoma cells in response to high-frequency stimulation (2 Hz or higher) (39).

Given the properties of RT neurons, especially their very high-frequency firing (up to 500 Hz), these cells might be more susceptible to CBZ inhibition compared to other neuron types such as CA1 pyramidal neurons, which fire at low-frequency (10 to 30 Hz) and exhibit minimal inhibition even at high CBZ concentrations (100 μM) (16). In addition, CBZ had variable effects on the firing behavior among three classes of GABAergic interneurons such as a basket cell (BC), a proximal dendritic targeting cell (PD), and an oriens lacunosum-moleculare (OLM) interneurons at very high rates (40, 41) in the rodent hippocampus (19). Despite these expectations, we actually found little effect of CBZ on high frequency burst firing. The effects of CBZ on RT firing was maximal in response to long-lasting, several seconds long, square pulse current injections, which simulate paroxysmal depolarization shifts (42–44), mimicking the electrical activity of an epileptic focus. Notably, this inhibitory effect disappears in response to pulse train stimulations (5 to 50 Hz) producing comparable number of total action potentials, confirming that it is not high frequency firing, per se, that engages CBZ block, but that is the sustained depolarization between action potentials. Thus, an epileptic-like plateau with sustained, seconds-long, depolarization of membrane potential to values positive of −60 mV is particularly effective in triggering use-dependent block. Note that high-frequency burst firing of RT neurons (Fig. 1*B*) does involve AP rates of several hundred Hz, but that each burst is limited to ~100 ms, which appears to be insufficient to engage use-dependent block (Fig. 1*E*, first 3 spikes). This is consistent with our findings that steady depolarization produces much greater block (Fig. 1*F*). In addition, CBZ has been shown to accelerate Nav slow inactivation and delay recovery from inactivation (45, 46). Given that at these concentrations, we saw no effect on individually evoked APs at baseline, the CBZ effects we see with prolonged AP trains, associated with long periods of sustained depolarization, likely involve accelerated slow inactivation. In contrast, burst firing for brief periods (~100 ms) may engage more transient sodium channel inactivation with less dependence on slow inactivation mechanisms that are more susceptible to use-dependent Nav block by CBZ. These properties of CBZ are likely to explain CBZ's preferential reduction of tonic over burst firing.

RT neurons provide both feedforward and feedback inhibition to excitatory TC neurons, with layer 6 corticothalamic (CT) inputs inducing feedforward inhibition of TC neurons (47–50). Reciprocal connectivity between TC and RT neurons generates 7 to 14 Hz spindle oscillations even without cortical input (51), suggesting that GABAergic output of RT to TC involves the generation of rhythmicity in the thalamus. A recent study demonstrated that impaired thalamic GABAergic transmission in NLG2 KO mice is correlated with spontaneous SWDs and behavioral arrest (34), consistent with the idea that CBZ effects, which also suppress GABAergic transmission at the RT-TC synapses could contribute to aggravation of absence seizures by this drug. RT neurons are heterogenous, roughly divided into two populations based on PV and SST expression,

Downloaded from https://www.pnas.org by STANFORD UNIVERSITY on August 1, 2025 from IP address 171.66.11.105.

each with distinct thalamocortical projections. PV-expressing RT neurons, with rhythmogenic properties mediated by robust expression of T-type calcium channels, mainly project to the sensory circuits of the VB thalamus, modulating somatosensory behavior and seizures (11), whereas SST-expressing RT neurons target the intralaminar (IL) thalamocortical nuclei and PF thalamus, influencing gamma rhythms and visual processing (12, 14). Considering the causal link between the activity of PV-expressing RT neurons and absence seizures, increased synaptic failure at PV-expressing RT-TC connections by CBZ might underlie its seizure-aggravating effects. In the thalamocortical circuit, cortical input to the sensory thalamus induces feed-forward inhibition of TC neurons via RT neurons during oscillations. Reduced cortico-RT projection strength in GluA4-deficient ($Gria4^{-/-}$) mice disrupts the cortico-thalamo-cortical system, resulting in spontaneous SWD (49). Future studies should examine CBZ's impact on other synapses within thalamo-cortical circuits to clarify its role in aggravating absence seizures. Furthermore, as previously proposed, intra-RT synapses (52, 53) might contribute to absence seizure under conditions where intra-RT inhibition is disrupted. For instance, an increase in inhibitory input to RT neurons is correlated with reduction in the duration and power of oscillations, highlighting the critical role of intra-RT inhibition in modulating thalamocortical network activity (54). Intra-RT synapses appear to be more susceptible to failure than RT-TC synapses (15), perhaps due to known differences in axonal branching and caliber (55). Thus, intra-RT synapses might be particularly sensitive to CBZ. Unfortunately, while we did observe intra-RT synaptic responses in some RT cell recordings, we were not able to maintain stable, long-term recordings to directly test this hypothesis. Nonetheless, we anticipate that CBZ's influence on intra-RT synapses would parallel, or perhaps its effects on the RT-TC synapses.

The reduced locomotor activity induced by CBZ in $SCN8a^{med/+}$ mice could result from two actions, either an increase in behavioral absences, and associated freezing (56, 57), or through direct changes in motor function. The effects are most likely due to increases in behavioral absences, as heterozygous loss of function ($Scn8a^{\pm}$) mice have no motor deficits as measured with the rotarod test (58). Further, CBZ had no effect on open field behavior in WT mice, suggesting no direct influence of CBZ on motor behaviors.

In conclusion, this study elucidates mechanisms by which CBZ aggravates absence seizures, particularly through its selective inhibition of tonic firing in RT neurons and suppression of GABAergic transmission. Our findings demonstrate that CBZ further aggravates the preexisting reduction in tonic firing in $SCN8a^{med/+}$ mouse, which correlates with increased seizure frequency and duration, as well as reduced locomotor activity. This study sheds light on how CBZ alters RT neuron firing and GABAergic transmission, providing a clearer understanding of its paradoxical effect on absence seizures. Future research should aim to explore the effect of CBZ on other thalamic cell types that contribute to rhythmicity within thalamocortical circuits.

Materials and Methods

Animals. WT mice (C57BL/6 J) and hemizygous VGAT-ChR2 mice (VGAT-mhChR2-YFP, Jax stock#: 014548), parvalbumin (PV)-Cre knock-in mice (PV-Cre, Jax Stock#: 008069), and somatostatin (SOM)-Cre Knock-in mice (SOM-Cre, Jax stock#: 013044) were obtained from Jackson Laboratory and bred with C57BL/6 J mice (Stock#: 000664). Mice with the heterozygous loss of function mutation (59) in *Scn8a* were purchased from the Jackson laboratory ($C3HeB/FeJ\text{-}Scn8a^{med/J}$, Stock#: 003798), referred to in this manuscript as $SCN8a^{med\pm}$. $SCN8a^{med\pm}$ mice were maintained on a C3HeB/FeJ background resulting in litters that were either $SCN8a^{med\pm}$ or $SCN8a^{WT}$. For optogenetic experiments in epileptic $SCN8a^{med\pm}$ mice (15), hemizygous VGAT-ChR2 mice were crossed with $SCN8a^{med\pm}$ mice. All pups were genotyped at postnatal day 21 using a commercial service (Transnetyx), and only mice of the desired genotypes were selected and randomly assigned to experimental groups. All mice were maintained on a reverse 12 h dark/light cycle, and all experiments occurred during their active cycle. Males and females were used in all experiments and were 2 to 6 mo of age. No experimental differences due to sex were observed. Food and water were available ad libitum. All experiments were approved by the Stanford Administrative Panel on Laboratory Animal Care (APLAC, Protocol #12363) and were performed in accordance with the National Institute of Health guidelines.

In Vitro Slice Electrophysiology. Mice were anesthetized using pentobarbital sodium (i.p., 55 mg/kg) and brains were carefully removed and placed in a cold (~4 °C) oxygenated (95% O_2/5%CO_2) sucrose-based slicing solution containing (in mM): 234 sucrose, 11 glucose, 26 $NaHCO_3$, 2.5 KCl, 1.25 NaH_2PO_4, 10 $MgSO_4$, and 0.5 $CaCl_2$ (310 mOsm). Horizontal slices (270 μm) containing RT and TC regions were sectioned using a vibratome (VT1200, Leica) and incubated in an interface chamber (Brain Slice Keeper 4, AutoMate Scientific, Berkeley, California) and continuously oxygenated in warm (~32 °C) artificial cerebrospinal fluid (ACSF) containing (in mM): 10 glucose, 26 $NaHCO_3$, 2.5 KCl, 1.25 $NaHPO_4$, 2 $MgSO_4$, 2 $CaCl_2$, and 126 NaCl (290 to 300 mOsm) for an hour and then transferred to room temperature (~21 to 23 °C) for at least an hour prior to recording. Whole-cell patch clamp of RT neurons was conducted using borosilicate glass patch pipettes (4 to 6 MΩ) filled with intracellular solution containing the following in mM: 126 K-gluconate, 4 KCl, 2 Mg-ATP, 0.3 GTP-Tris, 10 phosphocreatine, and the pH was adjusted to 7.4 using KOH (290 mOsm).

For current-clamp recordings of RT neurons, cells were held at a membrane potential of approximately –70 mV with steady intracellular current throughout the recording. Experiments were performed in the presence of Kynurenic acid (1 mM) and Gabazine (SR-95531, 10 μM) to block fast excitatory and inhibitory synaptic transmission, respectively. Pipette capacitance was compensated and the bridge was balanced. Evoked action potentials (APs) were elicited by injecting 1-s-duration current steps of increasing amplitude. AP traces were further analyzed and first and second derivatives (dV/dt and d^2V/dt^2, respectively) were calculated using pClampfit 10.7 and customized MATLAB (MathWorks) code. For voltage-clamp recordings of inhibitory synaptic events that include optogenetically evoked IPSCs (oIPSCs), the pipette solution contained (in mM): 135 CsCl, 10 HEPES, 10 EGTA, 2 $MgCl_2$, 5 QX-314, and pH adjusted to 7.4 with CsOH (290 mOsm). Membrane potential was held at −70 mV and signals were recorded using a Multiclamp 700A amplifier with pClamp 10.7 software (Axon Instruments, San Jose, CA), at a sampling rate of 50 kHz and low-pass filtered at 10 kHz. oIPSCs were detected using custom software (Wdetecta, JRH). oIPSCs were blocked by bath application of 20 μM Gabazine at the holding potential of –70 mV and were not detectable at –5 mV, the expected reversal potential of Cl^-. We excluded data obtained from unstable recordings in which 1) the series resistance increased by >20% from an initial value, or 2) holding current changed by more than 100 pA.

EEG. $SCN8a^{WT}$ or $SCN8a^{med\pm}$ mice aged 2 to 6 mo were used for EEG recordings. Mice were anesthetized using isoflurane for the duration of the EEG implant procedure. Under anesthesia, the skull was exposed, and small burr holes on both sides were carefully drilled at specific coordinates for electrode placement. Sterilized gold pins were located within each of the skull burr holes with the pins just touching the dura, and then glued in place. A reference electrode was placed in the cerebellum. After electrode placement, mice were allowed to recover for at least 3 d in their home cages to ensure stable electrode integration. EEG recordings were conducted in a quiet, controlled environment during the active cycle of the mice. For EEG data acquisition, mice were connected to an Open Ephys/Intan headstage recording system via lightweight and flexible cables. EEG signals were amplified and filtered at 2 kHz. The continuous EEG signals were recorded for 20 min as a baseline. After i.p. injection of vehicle or CBZ (15 mg/kg), EEG signals were recorded for 40 min, with the first 20 min of acclimatization time not included in the analysis. Recorded EEG data were manually analyzed offline using MATLAB software with customized codes.

Open Field Test. $SCN8a^{WT}$ or $SCN8a^{med\pm}$ mice aged 2 to 6 mo were chosen for the open field test. Prior to the test, mice were acclimated to the testing room for at least 1 h to minimize environmental stressors. The open field test was conducted in a square arena (50 × 50 × 50 cm) with white walls. Each mouse was

Downloaded from https://www.pnas.org by STANFORD UNIVERSITY on August 1, 2025 from IP address 171.66.11.105.

gently placed in the center of the open field arena and habituated for 10 min. After injecting vehicle or CBZ (15 mg/kg) into each SCN8a^{WT} or SCN8a$^{med\pm}$ mice, the mouse was placed in the arena again. Locomotor activity was recorded for 40 min and the data from the first 20 min were excluded from analysis to allow time for brain penetration of the CBZ. To compare locomotor activity, we used the data from 20 to 40 min. Video-tracking was employed for accurate behavioral quantification. Locomotor activity (distance traveled) was recorded and analyzed using Python code.

Drugs. CBZ (Sigma, Cat. No. C4024) was dissolved in 10% dimethyl sulfoxide (DMSO) for in vitro slice recording and in a solution of 40% propylene glycol, 10% ethanol, and 50% saline for in vivo measurement. Kynurenic acid was dissolved in 10% DMSO, and GABAzine (SR 95531) was dissolved in water for slice recording to block ionotropic glutamate receptor and $GABA_A$ receptor, respectively. Equivalent solvent concentrations were included in control solutions. Ethosuximide (200 mg/kg) was dissolved in 0.3% Tween 80 (Sigma-Aldrich, ON, CA).

Quantification and Statistical Analysis. All bar graphs represent means, with error bars indicating ± SEM. Statistical analyses were performed using GraphPad Prism 9 (GraphPad Software, La Jolla, CA), Excel (Microsoft), and Custom MATLAB programs (MathWorks, Natick, MA). Paired Student's *t* test was used to compare recording before and after the application of 30 μM CBZ. Unpaired tests were used for group comparisons of SCN8a$^{med\pm}$ and their wild-type littermates. A P value of <0.05 was considered statistically significant. Statistical values are denoted as follows: $*P < 0.05$, $**P < 0.01$, $***P < 0.001$, and $****P < 0.0001$.

Data, Materials, and Software Availability. All data supporting this study are included in the manuscript and/or *SI Appendix*.

ACKNOWLEDGMENTS. We thank all current lab members for their feedback during the entire project. We thank Cameron Glick for managing mouse lines, laboratory equipment, and supplies. This work was supported by National Institute of Neurological Disorders and Stroke (NS034774, NS117150).

1. D. Talwar, M. S. Arora, P. K. Sher, EEG changes and seizure exacerbation in young children treated with carbamazepine. *Epilepsia* **35**, 1154–1159 (1994).
2. J. D. Liporace, M. R. Sperling, M. A. Dichter, Absence seizures and carbamazepine in adults. *Epilepsia* **35**, 1026–1028 (1994).
3. P. Gelisse *et al.*, Worsening of seizures by oxcarbazepine in juvenile idiopathic generalized epilepsies. *Epilepsia* **45**, 1282–1286 (2004).
4. A. Parmeggiani, E. Fraticelli, P. G. Rossi, Exacerbation of epileptic seizures by carbamazepine: Report of 10 cases. *Seizure* **7**, 479–483 (1998).
5. L. Liu *et al.*, The mechanism of carbamazepine aggravation of absence seizures. *J. Pharmacol. Experime. Ther.* **319**, 790–798 (2006).
6. N. M. Pires, M. J. Bonifácio, P. Soares-da-Silva, Carbamazepine aggravates absence seizures in two dedicated mouse models. *Pharmacol. Rep.* **67**, 986–995 (2015).
7. J. Huguenard, D. Prince, A novel T-type current underlies prolonged Ca(2+)-dependent burst firing in GABAergic neurons of rat thalamic reticular nucleus. *J. Neurosci.* **12**, 3804–3817 (1992).
8. C. L. Cox, J. R. Huguenard, D. A. Prince, Nucleus reticularis neurons mediate diverse inhibitory effects in thalamus. *Proc. Natl. Acad. Sci. U.S.A.* **94**, 8854–8859 (1997).
9. C. L. Cox, J. R. Huguenard, D. A. Prince, Heterogeneous axonal arborizations of rat thalamic reticular neurons in the ventrobasal nucleus. *J. Comp. Neurol.* **366**, 416–430 (1996).
10. M. M. Halassa *et al.*, Selective optical drive of thalamic reticular nucleus generates thalamic bursts and cortical spindles. *Nat. Neurosci.* **14**, 1118–1120 (2011).
11. A. Clemente-Perez *et al.*, Distinct thalamic reticular cell types differentially modulate normal and pathological cortical rhythms. *Cell Rep.* **19**, 2130–2142 (2017).
12. M. S. Hoseini *et al.*, Gamma rhythms and visual information in mouse V1 specifically modulated by somatostatin+ neurons in reticular thalamus. *eLife* **10**, e61437 (2021).
13. M. Abdelaal *et al.*, Dysfunction of parvalbumin-expressing cells in the thalamic reticular nucleus induces cortical spike-and-wave discharges and an unconscious state. *Brain Commun.* **4**, fcac010 (2022).
14. S. Ahrens *et al.*, ErbB4 regulation of a thalamic reticular nucleus circuit for sensory selection. *Nat. Neurosci.* **18**, 104–111 (2015).
15. C. D. Makinson *et al.*, Regulation of thalamic and cortical network synchrony by Scn8a. *Neuron* **93**, 1165–1179.e6 (2017).
16. M. C. Evans, K. A. Dougherty, Carbamazepine-induced suppression of repetitive firing in CA1 pyramidal neurons is greater in the dorsal hippocampus than the ventral hippocampus. *Epilepsy Res.* **145**, 63–72 (2018).
17. G. Morris *et al.*, Activity clamp provides insights into paradoxical effects of the anti-seizure drug carbamazepine. *J. Neurosci.* **37**, 5484–5495 (2017).
18. M. Wolff *et al.*, Amitriptyline and carbamazepine utilize voltage-gated ion channel suppression to impair excitability of sensory dorsal horn neurons in thin tissue slice: An in vitro study. *Neurosci. Res.* **109**, 16–27 (2016).
19. L. Pothmann *et al.*, Function of inhibitory micronetworks is spared by Na+ channel–acting anticonvulsant drugs. *J. Neurosci.* **34**, 9720–9735 (2014).
20. G. Grześk *et al.*, Therapeutic drug monitoring of carbamazepine: A 20-year observational study. *JCM* **10**, 5396 (2021).
21. I. Kovačević, J. Parojčić, I. Homšek, M. Tubić-Grozdanis, P. Langguth, Justification of biowaiver for carbamazepine, a low soluble high permeable compound, in solid dosage forms based on IVIVC and gastrointestinal simulation. *Mol. Pharm.* **6**, 40–47 (2009).
22. A. F. Ambrósio *et al.*, Carbamazepine inhibits L-type Ca2+ channels in cultured rat hippocampal neurons stimulated with glutamate receptor agonists. *Neuropharmacology* **38**, 1349–1359 (1999).
23. T. Budde, T. Munsch, H. C. Pape, Distribution of L-type calcium channels in rat thalamic neurones. *Eur. J. Neurosci.* **10**, 586–597 (1998).
24. R. S. Zucker, W. G. Regehr, Short-term synaptic plasticity. *Annu. Rev. Physiol.* **64**, 355–405 (2002).
25. A. Beydoun *et al.*, Current role of carbamazepine and oxcarbazepine in the management of epilepsy. *Seizure* **83**, 251–263 (2020).
26. D. Schmidt, C. E. Elger, What is the evidence that oxcarbazepine and carbamazepine are distinctly different antiepileptic drugs?. *Epilepsy Behav.* **5**, 627–635 (2004).
27. A. Dhuna, A. Pascual-Leone, D. Talwar, Exacerbation of partial seizures and onset of nonepileptic myoclonus with carbamazepine. *Epilepsia* **32**, 275–278 (1991).
28. O. C. Snead, L. C. Hosey, Exacerbation of seizures in children by carbamazepine. *N. Engl. J. Med.* **313**, 916–921 (1985).
29. S. Thankachan *et al.*, Thalamic reticular nucleus parvalbumin neurons regulate sleep spindles and electrophysiological aspects of schizophrenia in mice. *Sci. Rep.* **9**, 3607 (2019).
30. R. E. Strandjord, S. I. Johannessen, Single-drug therapy with carbamazepine in patients with epilepsy: Serum levels and clinical effect. *Epilepsia* **21**, 655–752 (1980).
31. H. A. Spiller, E. P. Krenelok, E. Cookson, Carbamazepine overdose: A prospective study of serum levels and toxicity. *J. Toxicol. Clin. Toxicol.* **28**, 445–458 (1990).
32. J. Hojer, H. O. Malmlund, A. Berg, Clinical features in 28 consecutive cases of laboratory confirmed massive poisoning with carbamazepine alone. *J. Toxicol. Clin. Toxicol.* **31**, 449–458 (1993).
33. A. C. Lu *et al.*, Nonlinearities between inhibition and T-type calcium channel activity bidirectionally regulate thalamic oscillations. *eLife* **9**, e59548 (2020).
34. F. Cao *et al.*, Neuroligin 2 regulates absence seizures and behavioral arrests through GABAergic transmission within the thalamocortical circuitry. *Nat. Commun.* **11**, 3744 (2020).
35. L. Jia, T. E. Eroglu, R. Wilders, A. O. Verkerk, H. L. Tan, Carbamazepine increases the risk of sudden cardiac arrest by a reduction of the cardiac sodium current. *Front. Cell Dev. Biol.* **10**, 891996 (2022).
36. S. Jo, B. P. Bean, Sidedness of carbamazepine accessibility to voltage-gated sodium channels. *Mol. Pharmacol.* **85**, 381–387 (2014).
37. G. Reckziegel, H. Beck, J. Schramm, B. W. Urban, C. E. Elger, Carbamazepine effects on Na^+ currents in human dentate granule cells from epileptogenic tissue. *Epilepsia* **40**, 401–407 (1999).
38. M. Uebachs *et al.*, Efficacy loss of the anticonvulsant carbamazepine in mice lacking sodium channel subunits via paradoxical effects on persistent sodium currents. *J. Neurosci.* **30**, 8489–8501 (2010).
39. M. Willow, T. Gonoi, W. A. Catterall, Voltage clamp analysis of the inhibitory actions of diphenylhydantoin and carbamazepine on voltage-sensitive sodium channels in neuroblastoma cells. *Mol. Pharmacol.* **27**, 549–558 (1985).
40. T. F. Freund, G. Buzsáki, Interneurons of the hippocampus. *Hippocampus* **6**, 347–470 (1996).
41. Petilla Interneuron Nomenclature Group *et al.*, Petilla terminology: nomenclature of features of GABAergic interneurons of the cerebral cortex. *Nat. Rev. Neurosci.* **9**, 557–568 (2008).
42. D. A. Prince, M. Avoli, "The paroxysmal depolarizing shift: The first cellular marker of focal epileptogenesis" in *Jasper's Basic Mechanisms of the Epilepsies*, J. L. Noebels, M. Avoli, M. A. Rogawski, A. Vezzani, A. V. Delgado-Escueta, Eds. (Oxford University Press, 5th Ed., 2024).
43. M. Hotka, H. Kubista, The paroxysmal depolarization shift in epilepsy research. *Int. J. Biochem. Cell Biol.* **107**, 77–81 (2019).
44. A. K. Tryba *et al.*, Role of paroxysmal depolarization in focal seizure activity. *J. Neurophysiol.* **122**, 1861–1873 (2019).
45. J.-E. Han, J.-H. Cho, M. Nakamura, M.-G. Lee, I.-S. Jang, Effect of carbamazepine on tetrodotoxin-resistant Na+ channels in trigeminal ganglion neurons innervating to the dura. *Korean J. Physiol. Pharmacol.* **22**, 649–660 (2018).
46. P. L. Sheets, C. Heers, T. Stoehr, T. R. Cummins, Differential block of sensory neuronal voltage-gated sodium channels by lacosamide [(2R)-2-(acetylamino)-N-benzyl-3-methoxypropanamide], lidocaine, and carbamazepine. *J. Pharmacol. Exp. Ther.* **326**, 89–99 (2008).
47. S. R. Crandall, S. J. Cruikshank, B. W. Connors, A corticothalamic switch: Controlling the thalamus with dynamic synapses. *Neuron* **86**, 768–782 (2015).
48. W. Guo, A. R. Clause, A. Barth-Maron, D. B. Polley, A corticothalamic circuit for dynamic switching between feature detection and discrimination. *Neuron* **95**, 180–194.e5 (2017).
49. J. T. Paz *et al.*, A new mode of corticothalamic transmission revealed in the Gria4(-/-) model of absence epilepsy. *Nat. Neurosci.* **14**, 1167–1173 (2011).
50. N. Hádinger *et al.*, Region-selective control of the thalamic reticular nucleus via cortical layer 5 pyramidal cells. *Nat. Neurosci.* **26**, 116–130 (2023).
51. M. Steriade, M. Deschênes, L. Domich, C. Mulle, Abolition of spindle oscillations in thalamic neurons disconnected from nucleus reticularis thalami. *J. Neurophysiol.* **54**, 1473–1497 (1985).
52. C. Deleuze, J. R. Huguenard, Distinct electrical and chemical connectivity maps in the thalamic reticular nucleus: Potential roles in synchronization and sensation. *J. Neurosci.* **26**, 8633–8645 (2006).
53. Y.-W. Lam, C. S. Nelson, S. M. Sherman, Mapping of the functional interconnections between thalamic reticular neurons using photostimulation. *J. Neurophysiol.* **96**, 2593–2600 (2006).
54. C. M. Schofield, M. Kleiman-Weiner, U. Rudolph, J. R. Huguenard, A gain in $GABA_A$ receptor synaptic strength in thalamus reduces oscillatory activity and absence seizures. *Proc. Natl. Acad. Sci. U. S. A.* **106**, 7630–7635 (2009).
55. M. V. Sanchez-Vives, T. Bal, D. A. McCormick, Inhibitory interactions between perigeniculate GABAergic neurons. *J. Neurosci.* **17**, 8894–8908 (1997).
56. M. Vergnes *et al.*, Spontaneous paroxysmal electroclinical patterns in rat: A model of generalized non-convulsive epilepsy. *Neurosci. Lett.* **33**, 97–101 (1982).
57. H. Blumenfeld, "Consciousness and epilepsy: why are patients with absence seizures absent?" in *Progress in Brain Research, The Boundaries of Consciousness: Neurobiology and Neuropathology*, S. Laureys, Ed. (Elsevier, 2005), pp. 271–603.
58. B. C. McKinney, C. Y. Chow, M. H. Meisler, G. G. Murphy, Exaggerated emotional behavior in mice heterozygous for the sodium channel Scn8a (Nav1.6). *Genes Brain Behav.* **7**, 629–638 (2008).
59. D. C. Kohrman, M. R. Smith, A. L. Goldin, J. Harris, M. H. Meisler, A missense mutation in the sodium channel Scn8a is responsible for cerebellar ataxia in the mouse mutant jolting. *J. Neurosci.* **16**, 5993–5999 (1996).

Downloaded from https://www.pnas.org by STANFORD UNIVERSITY on August 1, 2025 from IP address 171.66.11.105.